Available online at www.CivileJournal.org

Civil Engineering Journal

(E-ISSN: 2476-3055; ISSN: 2676-6957)

Vol. 12, No. 06, June, 2026

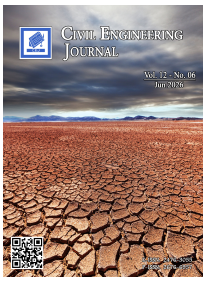

Optimization of Multiple Viscoelastic-Connected Tuned Mass Dampers Using Genetic Algorithm

Mohamed Bakr [1*], Tharwat A. Sakr [1], Mohamed Selim [1]

[1] *Structural Engineering Department, Faculty of Engineering, Zagazig University, Zagazig 44519, Egypt.*

Received 30 March 2026; Revised 24 May 2026; Accepted 27 May 2026; Published 01 June 2026

Abstract

Tuned Mass Dampers (TMDs) are widely used as effective supplementary damping devices for mitigating structural vibrations in high-rise buildings. Previous studies have primarily focused on TMD systems integrated with viscous dampers. This study proposes a Multiple Viscoelastic-Connected Tuned Mass Damper (MVTMD) system, in which adjacent TMD units are linked through viscoelastic elements that simultaneously contribute stiffness and damping, enhancing energy dissipation capacity and robustness against frequency variations. A comprehensive parametric investigation was conducted to identify the key parameters governing the performance of the proposed system. Owing to the complexity and interdependence of these parameters, a real-coded genetic algorithm was employed for multi-parameter optimization. The developed MATLAB model was validated against benchmark studies and showed good agreement with previously published results. The performance of the optimized MVTMD system was evaluated and compared with that of a conventional Single Tuned Mass Damper (STMD) under both harmonic and earthquake excitations. Under harmonic loading, the proposed MVTMD consistently outperformed the optimal STMD by producing flatter dynamic magnification factor (DMF) curves and achieving displacement reductions of 12.90%, 9.70%, and 15.50% for the five-, twenty-five-, and fifty-story buildings, respectively. Consistent improvements were also observed under earthquake excitations, confirming the system's superior vibration mitigation capability and robustness across a wide range of loading conditions.

Keywords: Structural Control; Buildings; Tuned Mass Damper; Viscoelastic; Earthquake; Wind; Optimization; Genetic Algorithm.

1. Introduction

Controlling structural vibrations in high-rise buildings has long posed a significant engineering challenge. Among various passive control strategies, the Tuned Mass Damper (TMD) has emerged as a reliable solution for mitigating undesirable oscillations. The TMD concept was initially proposed by Hermann Frahm in 1909, who created a mechanism to mitigate rolling motion and hull vibrations in ships [1]. This early innovation established the basis for the use of TMDs in mitigating structural vibrations in buildings. Later, in 1928, J.P. Den Hartog and J. Ormondroyd provided a theoretical foundation for TMDs, detailing optimal tuning and damping parameters for passive vibration control systems [2]. A tuned mass damper (TMD) generally comprises a secondary mass-spring-damper system affixed to a primary structure. When the structure undergoes vibrations, the TMD oscillates in opposition to the structural motion, thus dissipating energy and diminishing the amplitude of oscillations [3]. One of the most notable implementations of a Tuned Mass Damper (TMD) is in the Taipei 101 skyscraper in Taiwan. This 660-ton pendulum, consisting of solid steel plates and suspended by eight cables between the 87th and 92nd floors, accounts for about 0.26% of the building's total weight, making it the largest of its kind globally [4]. The damper has a significant effect on mitigating unwanted dynamic

* Corresponding author: mbtageldin@zu.edu.eg

https://doi.org/10.28991/CEJ-2026-012-06-023

responses, reducing the building's motion by up to 40% during strong winds and seismic events [5]. Other prominent structures employing TMDs include the Shanghai Tower, Petronas Twin Towers, 432 Park Avenue, the CN Tower, the John Hancock Tower, and the Sydney Tower [6, 7]. These systems are designed to counteract lateral loads such as wind and earthquakes, enhancing the stability and occupant comfort of these tall buildings [8, 9].

Research on TMD performance and enhancement has progressed steadily, with Single Tuned Mass Dampers (STMDs) consistently demonstrating effective vibration control. Brock [10] proposed a technique for ascertaining suitable TMD parameters for undamped materials subjected to broadband harmonic stimulation. Snowdon [11] investigated the steady-state response of dynamic absorbers incorporating various forms of absorber damping. Crandall & Mark [12] illustrated the efficacy of TMDs in mitigating SDOF vibrations induced by white noise base excitation. Falcon et al. [13] proposed a graphical approach to optimize an absorber with limited damping, applied to a damped primary system. Warburton & Ayorinde [14] derived optimal TMD parameters for SDOF systems under various loading conditions and tabulated optimal values for specific mass and damping ratios. Thompson [15] derived optimal TMD parameters for a damped, force-excited system and introduced a frequency locus method for their determination. Warburton [16] examined optimal TMD design for SDOF systems under various excitations, highlighting that the absorber mass should typically remain below 10% of the primary system's mass.

Tsai & Lin [17] addressed damped primary structures subjected to harmonic base excitation, demonstrating significant peak response reduction near resonance and providing numerical charts and empirical formulas for optimal parameter selection. Sadek et al. [18] established optimal TMD parameters for seismic loading, demonstrating that higher mass ratios enhance STMD effectiveness. Rana & Soong [19] conducted a landmark parametric study on STMDs under earthquake records and proposed a simplified design approach; their sensitivity analysis revealed that although increased mass and damping improve robustness against detuning, effectiveness diminishes in highly damped structures. Beyond classical analytical approaches, several metaheuristic optimization techniques have been employed to refine TMD performance. Leung & Zhang [20] applied a particle swarm optimization (PSO) algorithm to optimize the mass ratio, damping ratio, and tuning frequency of the passive system under various excitation conditions, Bekdaş & Nigdeli [21] demonstrated the effectiveness of harmony search for seismic applications. Hybrid genetic algorithms have also been used to optimize both placement and mechanical properties [22].

The concept of the Multiple Tuned Mass Damper (MTMD) was introduced by Xu & Igusa [23] and Yamaguchi & Hamporchai [24], employing several sub-oscillators with frequencies closely spaced. Their studies established that optimally designed MTMDs exhibit superior effectiveness and robustness compared to a single TMD of equivalent total mass, particularly across a wide range of damping ratios and under harmonic excitations. Kareem & Kline [25] showed that multiple smaller TMDs mounted on tall buildings enhance vibration control under wind and seismic loads, offering practical benefits such as broader frequency coverage, ease of installation, and reduced damper size. Li [26] and Li & Liu [27] demonstrated that optimized MTMD systems provide improved dynamic performance and robustness compared to STMD systems by minimizing the dynamic magnification factor (DMF) of the primary structure. Zuo & Nayfeh [28] formulated a decentralized static-output feedback approach for designing MTMDs attached to MDOF primary systems and introduced the MDOF-TMD configuration with both translational and rotational degrees of freedom. A novel optimal design theory was introduced for TMD-equipped buildings, overcoming the constraints of simpler methodologies and enabling wider applicability [29].

Mohebbi et al. [30] employed genetic algorithms to optimize MTMD parameters, reporting improved seismic performance with higher mass ratios under both near- and far-field excitations. Wang et al. [31] developed a multi-objective stochastic optimization method for MTMD systems to mitigate lateral–torsional seismic responses in eccentric buildings. A hybrid technique combining Particle Swarm Optimization and Grey Wolf Optimizer (PSO-GWO) has been employed to optimize STMD and MTMD configurations for nearby structures, with distributed MTMDs (d-MTMDs) enhancing performance [32]. Domizio et al. [33] investigated single and multiple TMD configurations for nonlinear structures under seismic loads, optimizing parameters with particle swarm optimization to enhance vibration mitigation. Inerter-based damping systems in buildings have been studied, with TID and MTMDI configurations optimized using a Cultural Algorithm and Escaping Bird Search algorithm, respectively, to achieve effective earthquake vibration mitigation [34, 35]. A multi-objective cuckoo optimization approach was proposed to determine the optimal MTMD parameters for reducing seismic responses in multi-story structures [36].

Several advanced TMD configurations have been explored, including systems utilizing rotational inertia double-tuned mass damper (RIDTMD) to enhance damping performance [37], while pounding TMDs (PTMDs) demonstrating significant acceleration reduction under sinusoidal input [38]. Adaptive TMDs (ATMDs) have proven effective under random excitation [39], and multi-story TMD configurations have been demonstrated to improve structural response to wind and seismic forces by augmenting story mass ratios and the quantity of damped floors [40]. Several studies have demonstrated the importance of accounting for soil–structure interaction (SSI) in the design and performance evaluation of tuned mass dampers (TMDs) and (MTMD) systems [41]. SSI can significantly influence structural dynamic responses and the effectiveness of vibration control under environmental loads [42, 43]. Moreover, recent improvements have

integrated TMDs with other structural control systems, such as inerters, markedly improving their vibration suppression effectiveness [33, 34]. A new type of TMD, the tuned tandem mass damper (TTMD), has been developed and shown to offer better stroke efficiency than traditional TMD systems [46]. An analytical method was established to ascertain the ideal parameters of viscoelastically damped tuned mass dampers (TMDs), demonstrating enhanced vibration control efficacy compared to traditional viscously damped systems [47]. A viscoelastic tuned inerter damper (VE TID) was developed to replace conventional stiffness and damping components with a cost-effective viscoelastic element, demonstrating through numerical analyses that it can efficiently and economically reduce seismic vibrations [48].

This study presents an innovative Multiple Viscoelastic-Connected Tuned Mass Damper (MVTMD) system designed to efficiently reduce structural vibrations induced by wind and seismic excitations. Figure 1 illustrates the principal TMD configurations Single TMD (STMD), Multiple TMD (MTMD), Tuned Tandem Mass Damper (TTMD), and the proposed MVTMD attached to a Single Degree of Freedom (SDOF) primary structure. Although STMD, MTMD, and TTMD systems have demonstrated effectiveness, their performance may deteriorate under parameter detuning and varying excitation characteristics, particularly when viscous interconnections provide energy dissipation without contributing additional stiffness. To address this limitation, the proposed MVTMD system incorporates viscoelastic interconnections, which provide combined stiffness and damping effects, enhanced energy dissipation capacity, and improved robustness against frequency variations. The MVTMD formulation, including the stiffness and damping distribution of the interconnected system, has been developed and verified. A comprehensive parametric study was conducted to evaluate and enhance the performance of the MVTMD system, and a real-coded genetic algorithm was employed to determine its optimal design parameters. Comparative analyses demonstrate that the proposed MVTMD configuration consistently outperforms the optimal STMD, offering superior vibration mitigation and improved robustness under varying excitation conditions, achieving flatter DMF curves and greater displacement reductions. The proposed system therefore offers a viable alternative to existing TMD configurations, contributing a tunable, robust, and effective solution for vibration control in modern civil engineering structures.

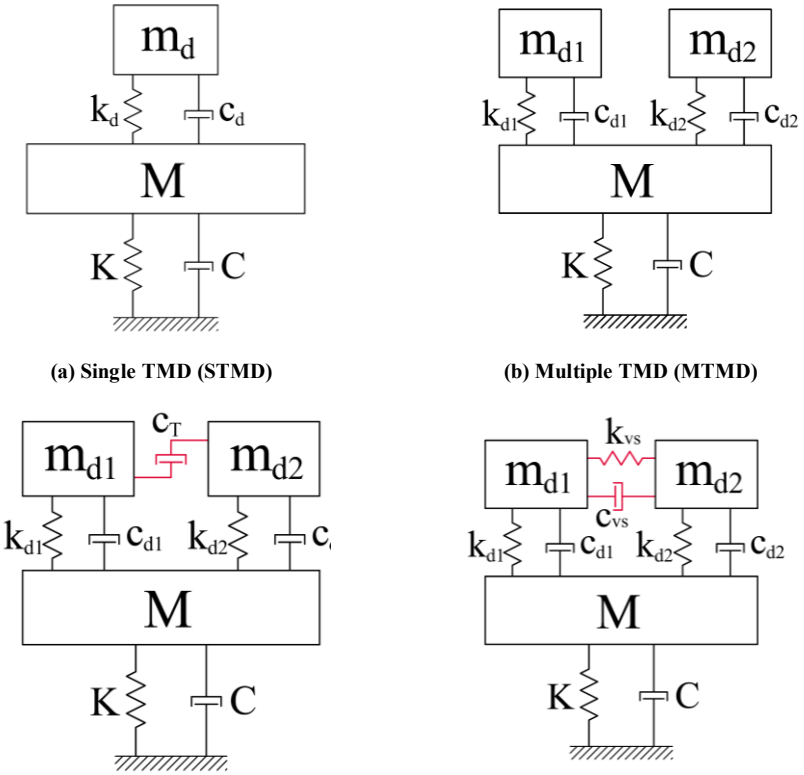

(a) Single TMD (STMD) **(b) Multiple TMD (MTMD)**

(c) Tuned Tandem Mass Damper (TTMD) **(d) Multiple Viscoelastic-Connected TMDs (MVTMD)**

Figure 1. Schematic of (a) Single TMD (STMD), (b) Multiple TMD (MTMD), (c) Tuned Tandem Mass Damper (TTMD), and (d) Multiple Viscoelastic-Connected TMDs (MVTMD) systems

2. Formulation of MVTMD

The schematic illustration shown in Figure 2 presents a building equipped with a multiple Viscoelastic-Connected Tuned Mass Dampers (MVTMD) system installed on the uppermost floor. The motion equation for the building equipped with a TMD can be expressed as follows:

$$M\ddot{x}+C\dot{x}+Kx = F \quad (1)$$

$$M = M_s+M_d \quad (2)$$

$$C = C_s+C_d \quad (3)$$

$$K = K_s+K_d \quad (4)$$

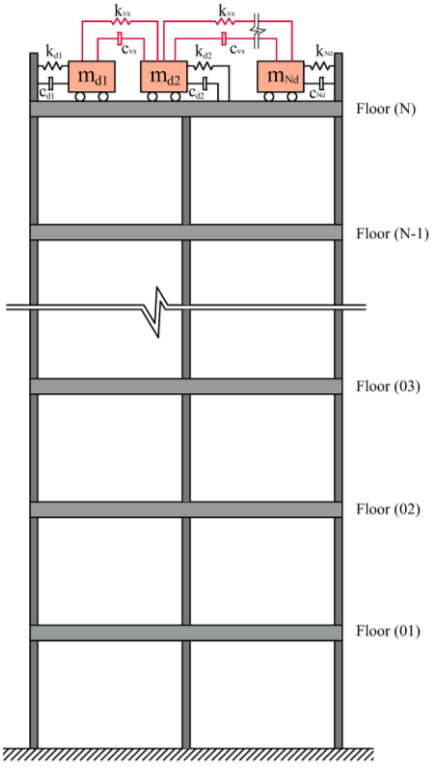

Figure 2. Model of building with Multiple Viscoelastic-Connected TMDs (MVTMD)

M, C, and K denote the mass, damping, and stiffness matrices, respectively. These matrices are defined as follows [49].

where M_s, C_s, and Ks represent the mass, damping, and stiffness matrices of the fundamental structure, respectively. The matrices M_d, Cd, and K_d represent the mass, damping, and stiffness matrices of the TMDs, respectively. The damping matrix of structure C is based on Rayleigh damping, which assumes the total damping is a linear combination of mass and stiffness effects, providing a simple approximation of damping in dynamic systems. It is defined as follows

$$C_s = \alpha M_s+\beta K_s \quad (5)$$

where, α and β are the mass and stiffness proportional damping coefficients derived from the two fundamental natural frequencies.

The building is modeled as a typical shear building consisting of N stories, where each story has a lumped mass m_i and stiffness k_i, with (i = 1, 2, . . ., N). The total number of dampers in this configuration is denoted by (j = 1, 2, . . ., N_d), with each damper characterized by a specific mass m_j, stiffness k_j, and damping coefficient c_j. The mass M, stiffness K, and damping C matrices for the building with the MVTMD system are delineated in Eqnations 6 to 8. The mass, stiffness, and damping of the j^{th} TMD are denoted by m_j, k_j and c_j, respectively. k_{vs}, c_{vs} denote the stiffness and the damping for the connecting viscoelastic dampers.

$$\mathbf{M} = \begin{bmatrix} m_i & 0 & \cdots & 0 & 0 & \cdots & 0 \\ 0 & m_{i+1} & \cdots & 0 & 0 & \cdots & 0 \\ \vdots & \vdots & \ddots & \vdots & \vdots & \cdots & \vdots \\ 0 & 0 & \cdots & m_n & 0 & \cdots & 0 \\ 0 & 0 & \cdots & 0 & m_j & \cdots & 0 \\ \vdots & \vdots & \cdots & \vdots & \vdots & \ddots & \vdots \\ 0 & 0 & \cdots & 0 & 0 & \cdots & m_{N_d} \end{bmatrix} \quad (6)$$

$$\mathbf{K}=\begin{bmatrix} k_i+k_{i+1} & -k_{i+1} & \cdots & 0 & 0 & 0 & \cdots & 0 \\ -k_{i+1} & k_{i+1} & \cdots & 0 & 0 & 0 & \cdots & 0 \\ \vdots & \vdots & \ddots & \vdots & \vdots & \cdots & \cdots & \vdots \\ 0 & 0 & \cdots & k_n+\sum_{j=1}^{N_d} k_j & -k_j & -k_{j+1} & \cdots & -k_{N_d} \\ 0 & 0 & \cdots & -k_j & k_j+k_{vs} & -k_{vs} & \cdots & 0 \\ 0 & 0 & \cdots & -k_{j+1} & -k_{vs} & k_{j+1}+2k_{vs} & \cdots & 0 \\ \vdots & \vdots & \cdots & \vdots & \vdots & \vdots & \ddots & \vdots \\ 0 & 0 & \cdots & -k_{N_d} & 0 & 0 & \cdots & k_{N_d}+k_{vs} \end{bmatrix} \tag{7}$$

$$\mathbf{C}=\begin{bmatrix} c_{11} & c_{12} & \cdots & 0 & 0 & 0 & \cdots & 0 \\ c_{21} & c_{22} & \cdots & 0 & 0 & 0 & \cdots & 0 \\ \vdots & \vdots & \ddots & \vdots & \vdots & \vdots & \cdots & \vdots \\ 0 & 0 & \cdots & c_{nn}+\sum_{j=1}^{N_d} c_j & -c_j & -c_{j+1} & \cdots & -c_{N_d} \\ 0 & 0 & \cdots & -c_j & c_j+c_{vs} & -c_{vs} & \cdots & 0 \\ 0 & 0 & \cdots & -c_{j+1} & -c_{vs} & c_{j+1}+2c_{vs} & \cdots & 0 \\ \vdots & \vdots & \cdots & \vdots & \vdots & \vdots & \ddots & \vdots \\ 0 & 0 & \cdots & -c_{N_d} & 0 & 0 & \cdots & c_{N_d}+c_{vs} \end{bmatrix} \tag{8}$$

The properties of each TMD number j^{th} in MVTMD can be formed as follows:

$$\mu=\frac{\sum_{j=1}^{N_d} m_j}{M^*} \tag{9}$$

$$\mu_1=\frac{m_1}{M^*} \tag{10}$$

μ, μ_1, and M^* are the mass ratio of the MVTMD system, the mass ratio of the first TMD, and the modal mass of the structure's fundamental frequency, respectively.

$$\omega_j=\omega_T\left[1-\left(j-\frac{N_d+1}{2}\right)\frac{\beta}{N_d-1}\right] \tag{11}$$

$$\omega_T=\frac{\sum_{j=1}^{N_d}\omega_j}{N_d} \tag{12}$$

$$\beta=\frac{\omega_1-\omega_{N_d}}{\omega_T} \tag{13}$$

$$f=\frac{\omega_T}{\omega_s} \tag{14}$$

where, ω_j, ω_T, and ω_s are the natural frequency of the j^{th} TMD, the average natural frequency of the entire TMD system, and the natural frequency corresponding to the structure's first mode, respectively. And β is the dimensionless frequency range of the MVTMD system, and f is the tuning ratio defined as the ratio of the average natural frequency of the TMD system to the structure's first mode shape natural frequency. The masses for each TMD are equal except for the first TMD, which has its own mass ratio, and the natural frequencies are equally distributed in the frequency range β around the average frequency ω_T [24]. Then the stiffness and the damping for each j^{th} TMD can be calculated as shown in the following equations.

$$K_j=m_j\omega_j^2 \tag{15}$$

$$C_j=2\zeta_j m_j\omega_j \tag{16}$$

Figure 3 depicts the traditional models of viscoelastic materials, including the Maxwell model, Kelvin model, Generalized Maxwell model, and Generalized Kelvin model [47]. The stiffness and damping of the connecting viscoelastic dampers are considered as a Kelvin model and defined as follows [50]:

$$\tau=K_{vs}x+C_{vs}\dot{x} \tag{17}$$

$$\gamma=\frac{K_{vs}}{K_j} \tag{18}$$

$$\eta=\frac{C_{vs}}{C_j} \tag{19}$$

where τ, γ, and η are the force, the stiffness ratio, and the damping ratio of the viscoelastic damper, respectively.

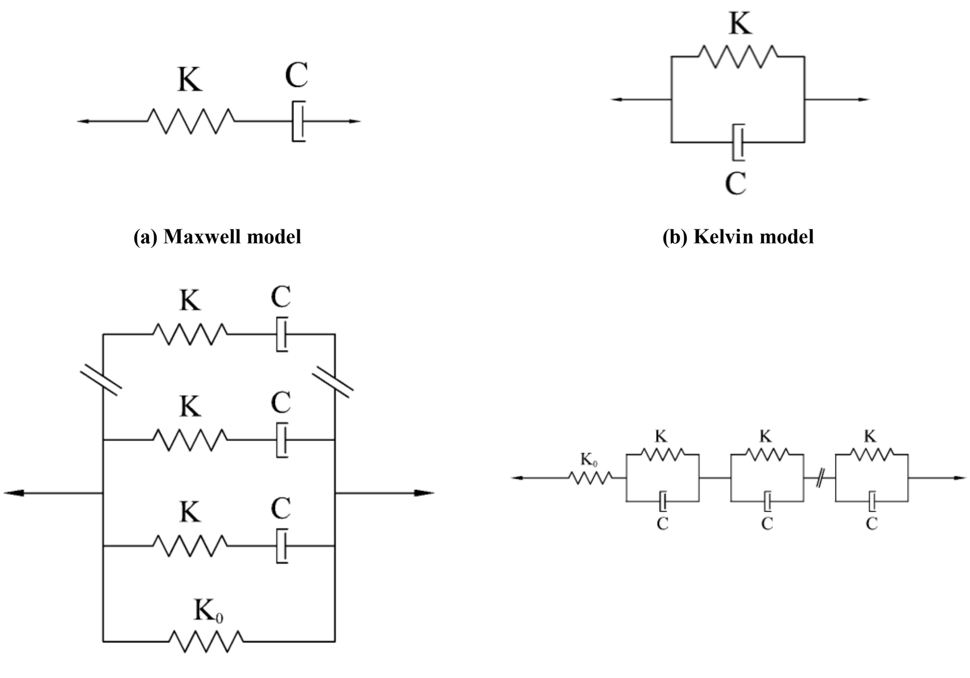

(a) Maxwell model **(b) Kelvin model**

(c) Generalized Maxwell model **(d) Generalized Kelvin model**

Figure 3. Classic viscoelastic material models: (a) Maxwell, (b) Kelvin, (c) Generalized Maxwell, and (d) Generalized Kelvin

The force vector F in Equation 1 represents two types of external excitations: the wind load F_w, modeled as a sinusoidal dynamic force to represent the fluctuating part of wind loading, and the earthquake load F_e, represented by a ground acceleration time history. The equation of motion is subsequently solved with the Newmark-β method [49], a time integration technique often employed in structural dynamics. The result indicates the displacement, velocity, and acceleration of the structure's nodes at each time period.

$$F_w = A\sin(\omega t)I \tag{20}$$

$$F_e = -MI\ddot{x}_g \tag{21}$$

where, A symbolizes an arbitrary amplitude of sinusoidal load, ω represents the angular frequency of wind excitations, I signifies the identity matrix, and $\ddot{x}_g$ indicates the ground acceleration.

3. Verification of Numerical Analysis

A benchmark 10-story shear building, previously examined by Arfiadi & Hadi [22], is utilized to test the numerical study and the developed MATLAB codes. The structural properties and tuned mass damper (TMD) configuration are replicated precisely, including a 115-ton damper situated on the 10th floor, with parameters Cd = 175.033 kN/m and Kd = 4540.369 kN/m, as detailed in Table 1. The basic mode shape calculated using the MATLAB algorithm aligns precisely with the reference findings, as seen in Table 2.

Table 1. Properties of the reference case [22]

Stories	Story stiffness (kN/m)	Story mass (ton)
1 – 2	1410587.50	572.90
3	1410587.50	567.60
4 – 6	1048724.20	562.30
7	1048724.20	548.30
8 – 9	1410587.50	535.32
10	1410587.50	489.30

Table 2. Comparison between the fundamental mode shapes obtained in this study and those of the reference case [22]

Source	This Study	Ref.
Fundamental mode shape	0	0
	0.09174	0.0917
	0.18182	0.1818
	0.2686	0.2686
	0.37883	0.3788
	0.48	0.48
	0.56967	0.5697
	0.64571	0.6457
	0.81979	0.8198
	0.9405	0.9405
	1.0	1.0

To validate the time integration method and evaluate the impact of the TMD, Figure 4 illustrates the lateral displacement response of the top level for both uncontrolled and controlled structures during the El Centro earthquake. The outcomes closely align with the reference instance, with the uncontrolled structure attaining a maximum displacement of 246.1 mm at 4.78 seconds, whereas the regulated structure decreased to 148.1 mm at 2.90 seconds. The maximum story drift distribution across the building height is illustrated in Figure 5, demonstrating consistency with the benchmark research. As shown in the Table 3, the relative error remains below 1–2% in all cases, thereby confirming the accuracy, and reliability of the proposed numerical approach.

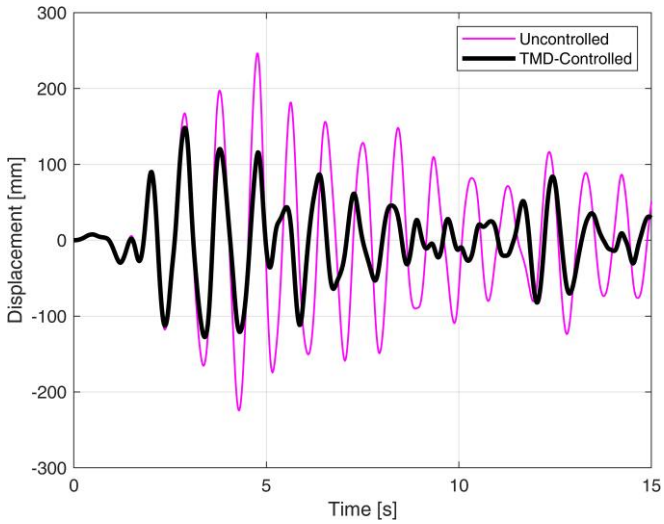

Figure 4. Time history of top-floor lateral displacement (verification example)

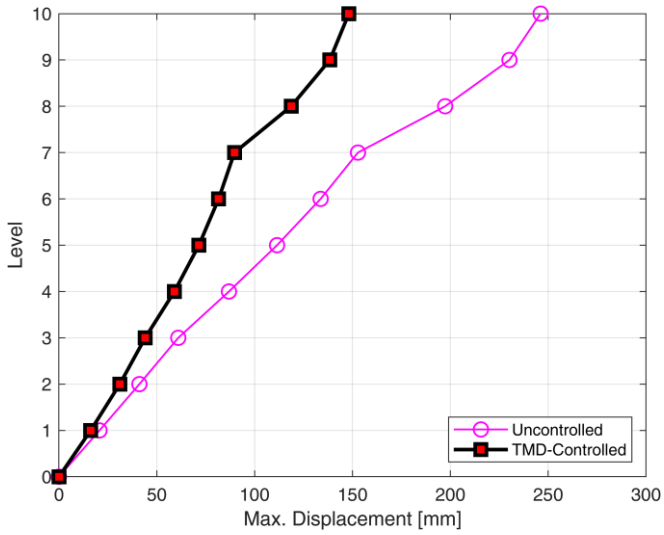

Figure 5. Distribution of maximum story displacement (verification example)

Table 3. Comparison between the displacement obtained in the present study and the reference results [22]

Story No	Uncontrolled (mm)	Uncontrolled Ref. (mm)	with TMD (mm)	With TMD Ref. (mm)
0	0.0	0.0	0.0	0.0
1	20.7	20.3	16.2	16.1
2	41.1	40.2	31.1	30.5
3	61.0	60.1	44.1	43.5
4	86.9	85.4	59.0	58.3
5	111.5	110.2	71.5	72.1
6	133.7	131.8	81.6	80.8
7	152.8	151.5	89.7	89.2
8	197.3	197.3	118.7	119.5
9	230.2	232	138.4	136.7
10	246.1	250	148.1	147.3

4. Results and Discussion

4.1. Parameters Affecting the Response of Buildings with MVTMD

The proposed MVTMD system includes eight design parameters; each of them can be tuned to minimize the dynamic magnification factor (DMF) under the corresponding loading scenario. These parameters are as follows: viscoelastic stiffness ratio (γ), viscoelastic damping ratio (η), tuning ratio (f), frequency range (β), total mass ratio (μ), first TMD mass ratio (μ_1), number of tuned mass dampers (NTMD), and damping ratio (ζ). For this numerical investigation, the structural properties are as follows: The building consists of five floors, each with a height of 4.0 m. The mass of each floor is 900 tons, and the stiffness of each floor is 1.20 × 106 kN/m. In parametric study, the building has a modal damping ratio $\zeta_s = 0.02$ and equipped with MVTMD, where only one parameter is varied at a time while all other parameters are maintained at the baseline values provided in Table 4. The MATLAB code runs for different excitation ratios (r) ranging from 0.6 to 1.40 to get the maximum DMF in each case for parametric study.

Table 4. MVTMD parameters used in the parametric study

Parameter	Value
Viscoelastic stiffness ratio (γ)	0.20
Viscoelastic damping ratio (η)	1.00
Tuning ratio (f)	1.00
Frequency range (β)	0.20
Total mass ratio (μ)	0.01
First TMD mass ratio (μ_1)	0.33
Number of TMDs (NTMD)	3
Damping ratio (ζ)	0.081

Figure 6 shows that increasing the viscoelastic stiffness ratio (γ) initially reduces the DMF, reaching an optimal, flattened frequency response at $\gamma = 0.25$. Beyond this point, further increases in γ lead to a rise in DMF, accompanied by distinct peak values. Similarly, Figure 7 demonstrates that increasing the viscoelastic damping ratio (η) also initially decreases the DMF, reaching an optimal minimum at $\eta = 1.00$. Further increases in η, however, result in an increase of the DMF, characterized by notable peaks in the frequency response. Figure 8 presents the effect of varying the tuning ratio (f) on the DMF for a structure with MVTMD. It can be observed that as f increases, the DMF initially decreases, achieving an optimal and minimal response at $f = 1.00$. Beyond this optimal tuning ratio, further increases in f cause the DMF to rise again, exhibiting distinct peak values.

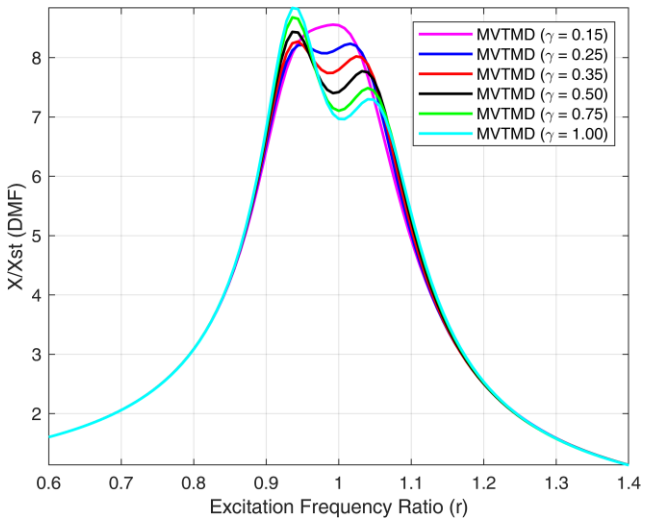

Figure 6. Relation between maximum dynamic magnification coefficient (DMF) and (r) for different viscoelastic stiffness ratios (γ)

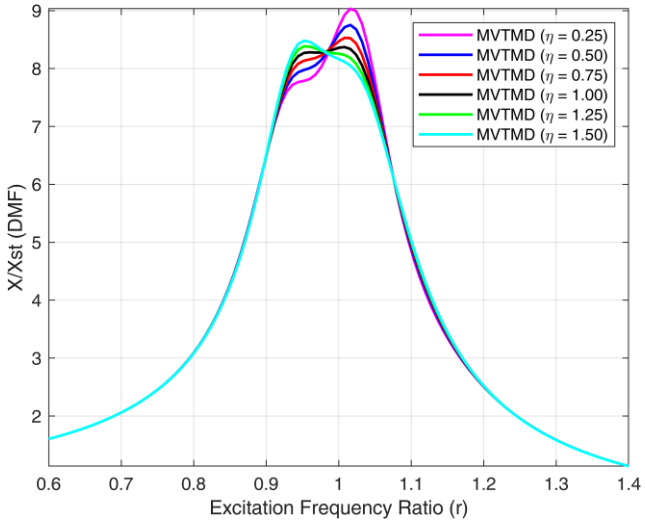

Figure 7. Relation between maximum dynamic magnification coefficient (DMF) and (r) for different viscoelastic damping ratios (η)

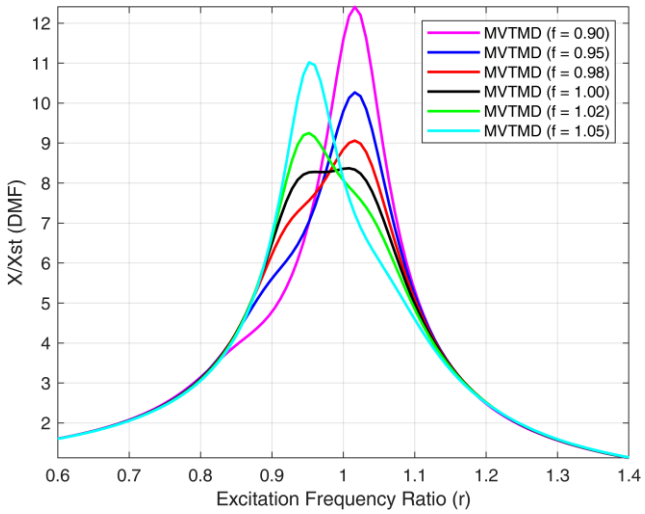

Figure 8. Relation between maximum dynamic magnification coefficient (DMF) and (r) for different tuning ratios (*f*)

Figure 9 illustrates how variations in the frequency range parameter (β) affect the DMF for a structure with MVTMD. The results show that increasing β initially leads to a reduction in DMF, reaching an optimal value at β = 0.20. Beyond this optimal point, further increases in β result in a rise of the DMF, characterized by clearly identifiable peak responses. Figure 10 illustrates the influence of the mass ratio (μ) on the (DMF) for a structure with an MVTMD. The figure indicates that DMF generally decreases as the mass ratio increases within the

investigated range. However, a selected mass ratio is identified at μ = 0.01, as it generates two closely spaced peaks, resulting in a more balanced and effective reduction in structural response. Figure 11 illustrates the effect of varying the first mass ratio (μ_1) on the dynamic magnification factor (DMF) for a total mass ratio of μ = 0.01. The figure demonstrates that for this smaller total mass ratio, optimal performance occurs when the TMD masses are equally distributed, corresponding to μ_1 = 0.33.

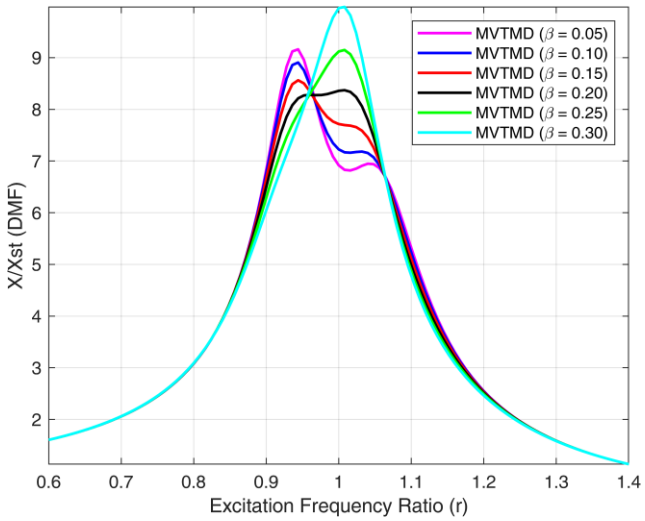

Figure 9. Relation between maximum dyna1mic magnification coefficient (DMF) and (r) for different frequency ranges (β)

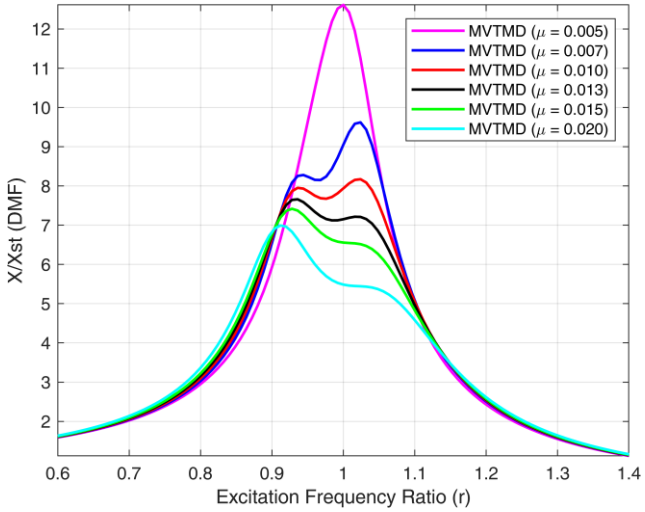

Figure 10. Relation between maximum dynamic magnification coefficient (DMF) and (r) for different mass ratios (μ)

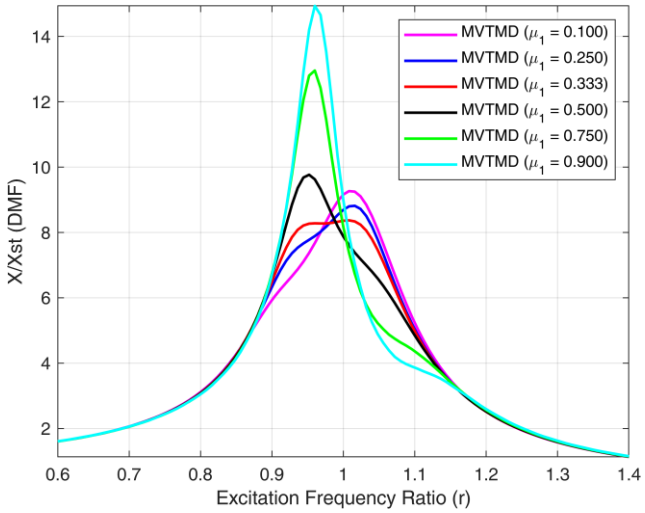

Figure 11. Relation between maximum dynamic magnification coefficient (DMF) and (r) for different first mass ratios (μ1) at (μ = 0.01)

Figure 12 illustrates the effect of varying the number of tuned mass dampers (NTMD) on the (DMF) for a structure with a (MVTMD). It is observed that DMF achieves its optimal minimum at NTMD = 3, beyond which it starts to increase again, exhibiting a distinct single peak. Figure 13 illustrates how variations in the damping ratio (ζ) for each TMD influence the DMF for the same structure with MVTMD. The results indicate that increasing ζ initially reduces DMF, achieving an optimal minimal response at ζ = 0.07. Beyond this damping ratio, further increases in ζ cause the DMF to rise again, exhibiting peaks with varying magnitudes.

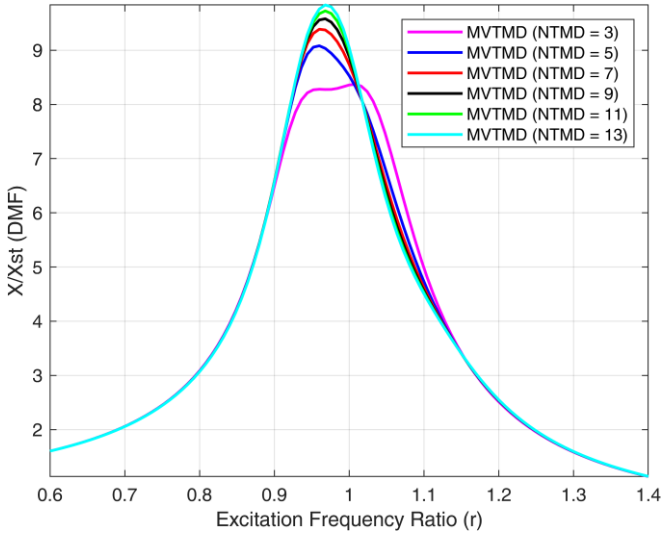

Figure 12. Relation between maximum dynamic magnification coefficient (DMF) and (r) for different numbers of TMD (NTMD)

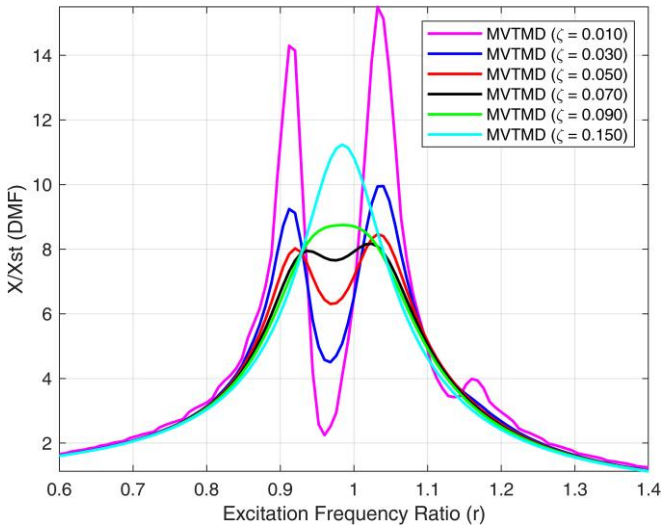

Figure 13. Relation between maximum dynamic magnification coefficient (DMF) and (r) for different damping ratios of TMDs (ζ)

The parametric study underscores critical insights into optimizing the MVTMD system for structural vibration mitigation. Specifically, an optimal viscoelastic stiffness ratio (γ = 0.25) and damping ratio (η = 1.00) yield significant reductions in DMF. Similarly, precise tuning (f = 1.00) and an appropriately selected frequency range (β = 0.20) are essential to minimize structural response as also reported in previous studies [51, 52]. Although increasing the mass ratio to μ = 0.02 further reduces the DMF, the most balanced response with uniform peak amplitudes is obtained at a moderate mass ratio (μ = 0.01). The distribution of individual TMD masses, represented by μ_1, tends toward equal partitioning at lower total mass ratios, as evidenced by μ_1 = 0.33 when μ = 0.01. Additionally, utilizing three tuned mass dampers (NTMD = 3) and selecting a damping ratio of ζ = 0.07 consistently result in optimal structural damping performance. It is to be noted that all parameters lead to optimized behaviour depend on the selected reference value of others and that if such reference parameters are changed, other findings can be reached. Overall, these findings highlight the strong interdependence among the governing parameters and provide practical guidance for the efficient implementation of MVTMD systems.

4.2. Genetic Algorithm Optimization of the MVTMD

Based on the parametric study, the complexity and interdependency of the optimization problem became evident due to the large solution space and the presence of multiple local minima. To efficiently navigate this complex optimization space, a genetic algorithm (GA) was employed. Specifically, a real-coded genetic algorithm was chosen due to its effectiveness in handling the continuous variables characteristic of MVTMD parameters. The chromosome structure adopted for the MVTMD optimization is illustrated in Figure 14, comprising eight parameters represented as real-valued genes.

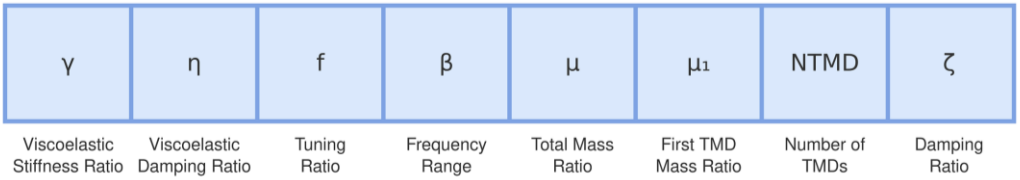

Figure 14. Chromosome structure for the real-coded GA, where each gene corresponds to the parameters of an MVTMD system

The genetic algorithm implemented follows a structured iterative process, as outlined below [53, 54]:

1. Initialization: Generate an initial population consisting of random candidate solutions (chromosomes), each defined by a vector of real-valued genes:

   $X = [x_1, x_2, \ldots, x_{50}]$

2. Fitness Evaluation: Evaluate the fitness of each chromosome using a predefined objective function, typically the maximum (DMF) under sinusoidal loading:

   $F(X) = DMF(X)$

3. Selection: Select chromosomes based on fitness scores using tournament selection, balancing diversity with a focus on promising solutions.

4. Crossover: Perform a real-coded intermediate crossover, defined by:

   $x_{offspring} = x_{(p)} + \alpha(x_{(q)} - x_{(p)})$

   where α is a random value between 0 and 1, and [p, q] represent parent chromosomes.

5. Mutation: Introduce variability by slightly perturbing the offspring genes using adaptive feasible mutation, ensuring offspring genes remain within the defined bounds or linear constraints.

6. Replacement and Elitism: Replace the current population with the offspring, retaining the best-performing solutions through elitism (with an elitism count set to 5).

7. Convergence Check: Repeat iterations until the stopping criterion (maximum generations or convergence threshold) is met.

A schematic overview of the described genetic algorithm procedure is presented in Figure 15.

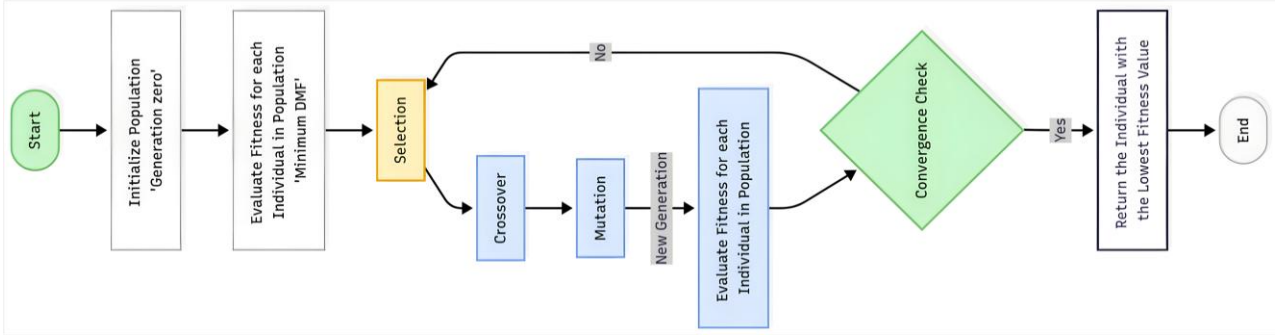

Figure 15. Flowchart illustrating the genetic algorithm procedure employed for optimizing the MVTMD parameters

The properties of the buildings analyzed for optimization are summarized in Table 5. Three building configurations were studied: a five-story, a twenty-five-story, and a fifty-story structure. For each structural configuration, an optimized (MVTMD) system was integrated based on genetic algorithm optimization.

Table 5. Main properties of studied buildings

Story No	Story stiffness (kN/m)	Story mass (ton)	Fundamental period (s)
5 story	1.20×10^6	900	0.60
25 story	1.80×10^6	1000	2.40
50 story	2.60×10^6	1200	4.33

Three optimization scenarios were considered: In the first approach, all eight parameters, including the mass ratio (μ), were optimized simultaneously, allowing the genetic algorithm to identify the most effective parameter combination. In the second approach, the optimization was performed using seven parameters, with the total mass ratio held constant at a commonly practical fixed value μ = 0.01 for both MVTMD and STMD. This approach assessed the impact of excluding μ from the optimization while optimizing the remaining parameters. Finally, in the third approach, the structure was optimized using six parameters, holding both the total mass ratio (μ = 0.01) for MVTMD and STMD and the number of tuned mass dampers (NTMD = 3) constants. Figure 16 illustrates the convergence of a genetic algorithm trial used to identify the optimal parameters of the proposed MVTMD system for the five-story building equipped with the MVTMD system. The detailed outcomes of the optimization are presented in Tables 6 to 7 and Figure 17 to Figure 25 for the five-story, twenty-five-story, and fifty-story buildings, respectively.

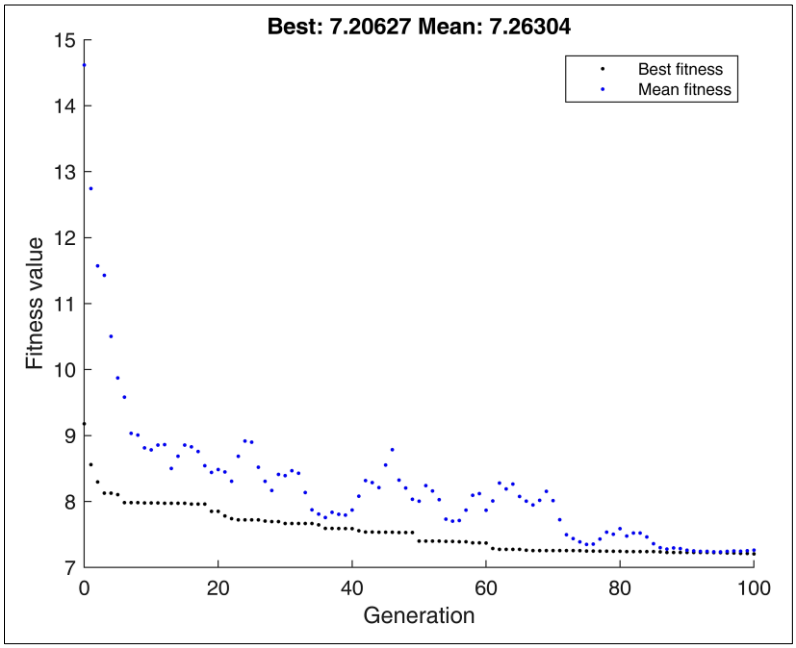

Figure 16. Fitness value versus generation number for the five-story building with the MVTMD system, optimized using six design parameters

Table 6. Optimal MVTMD system parameters derived from the genetic algorithm for the 5-story building

Trial	8 parameters	7 parameters	6 parameters
μ	0.02498	0.01	0.01
NTMD	11	10	3
μ_1	0.29173	0.37245	0.10096
f	0.93543	0.95988	1.01636
β	0.23759	0.15303	0.17223
ζ	0.07761	0.0490	0.04554
γ	0.30468	0.17116	0.0180
η	1.68879	1.4460	0.99895
DMF	5.06881	7.18713	7.20627

Table 7. Optimal MVTMD system parameters derived from the genetic algorithm for the 25-story building

Trial	8 parameters	7 parameters	6 parameters
μ	0.02494	0.01	0.01
NTMD	14	10	3
μ_1	0.26270	0.55490	0.49205
f	0.93676	0.94390	0.96765
β	0.21067	0.16491	0.19615
ζ	0.09814	0.05877	0.06797
γ	0.50243	0.36692	0.21929
η	0.48707	1.10180	1.39565
DMF	5.04419	7.19818	7.62178

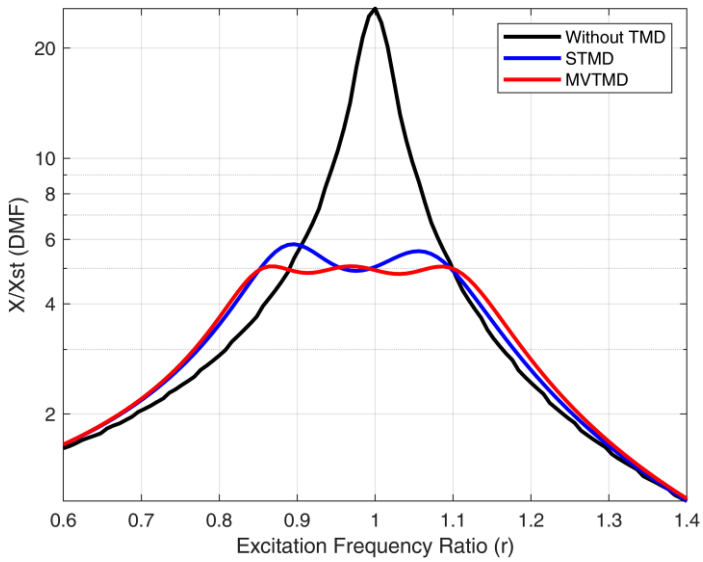

Figure 17. Relation between DMF and r for different TMD systems under eight-parameter optimization for a 5-story building

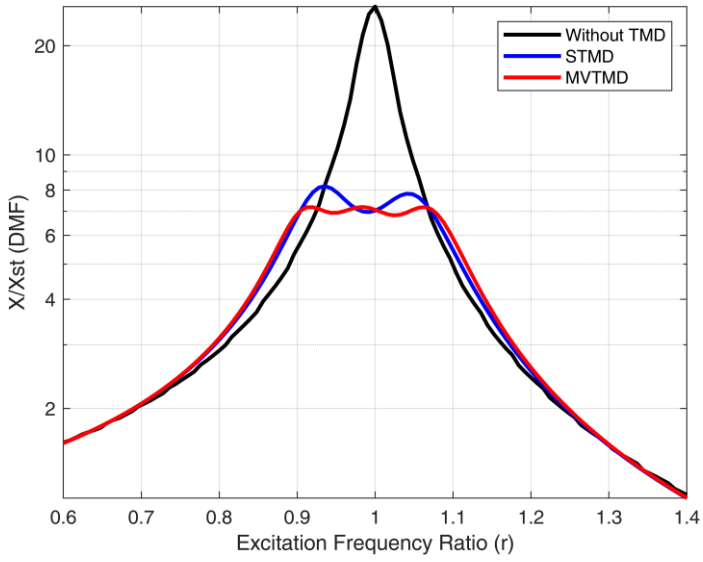

Figure 18. Relation between DMF and r for different TMD systems under seven-parameter optimization for a 5-story building

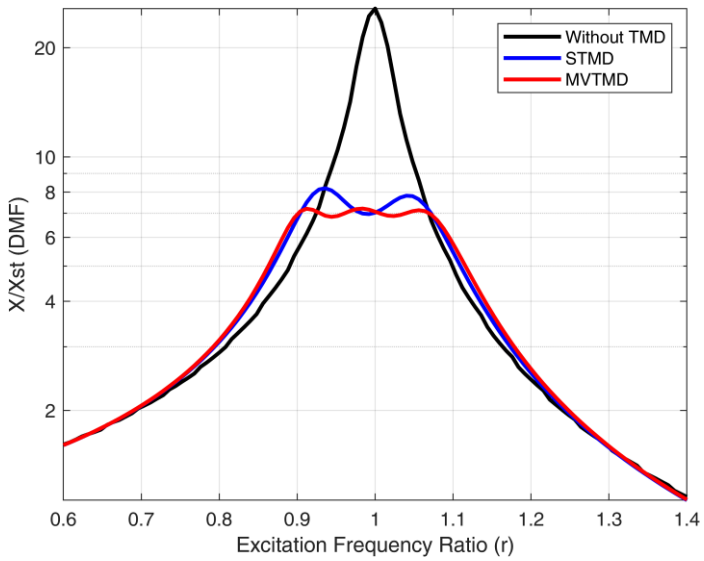

Figure 19. Relation between DMF and r for different TMD systems under six-parameter optimization for a 5-story building

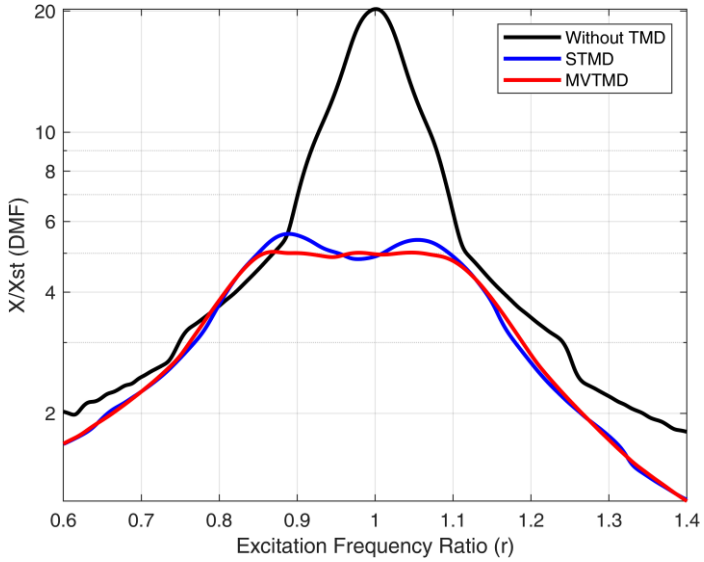

Figure 20. Relation between DMF and r for different TMD systems under eight-parameter optimization for a 25-story building

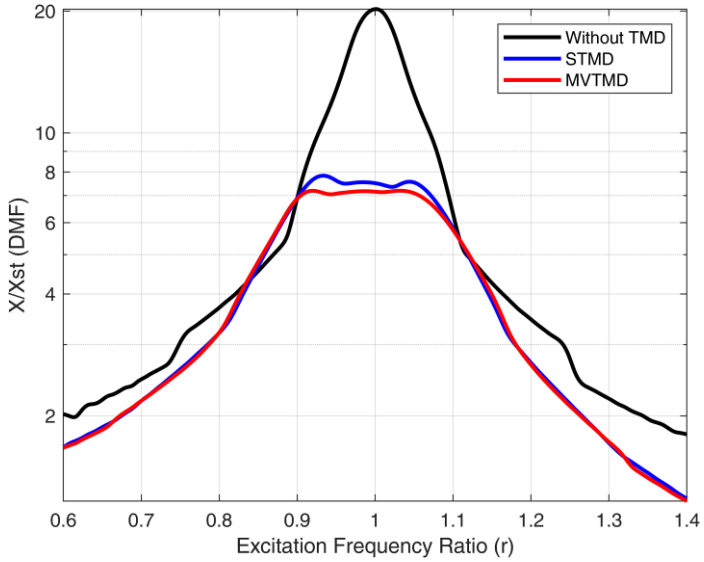

Figure 21. Relation between DMF and r for different TMD systems under seven-parameter optimization for a 25-story building

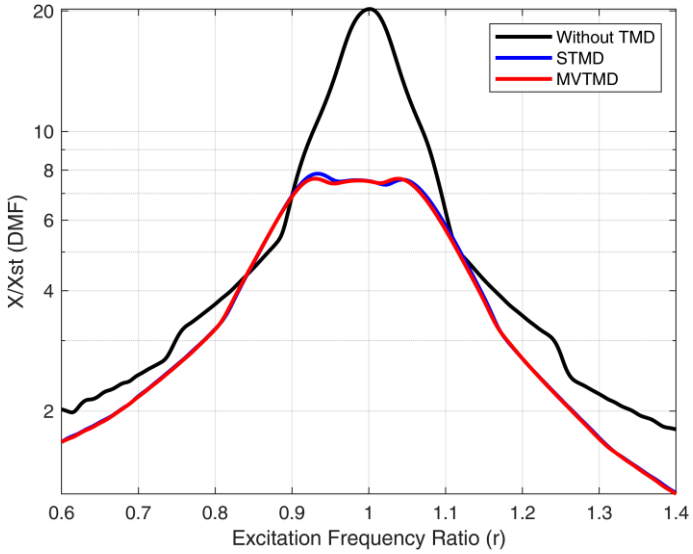

Figure 22. Relation between DMF and r for different TMD systems under six-parameter optimization for a 25-story building

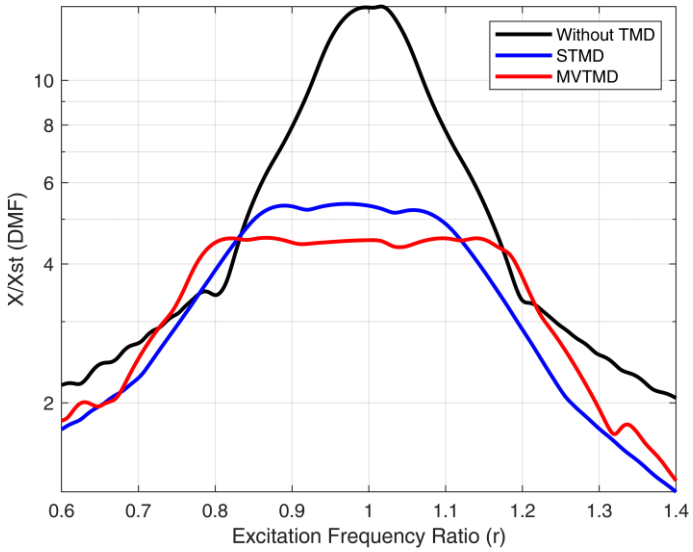

Figure 23. Relation between DMF and r for different TMD systems under eight-parameter optimization for a 50-story building

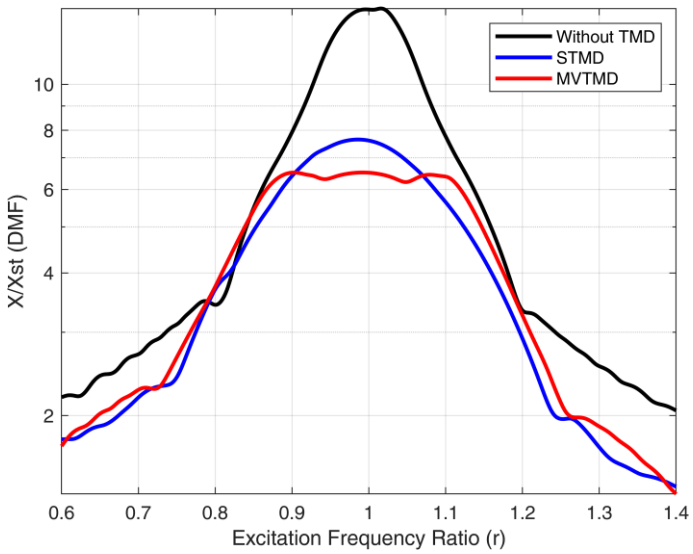

Figure 24. Relation between DMF and r for different TMD systems under seven-parameter optimization for a 50-story building

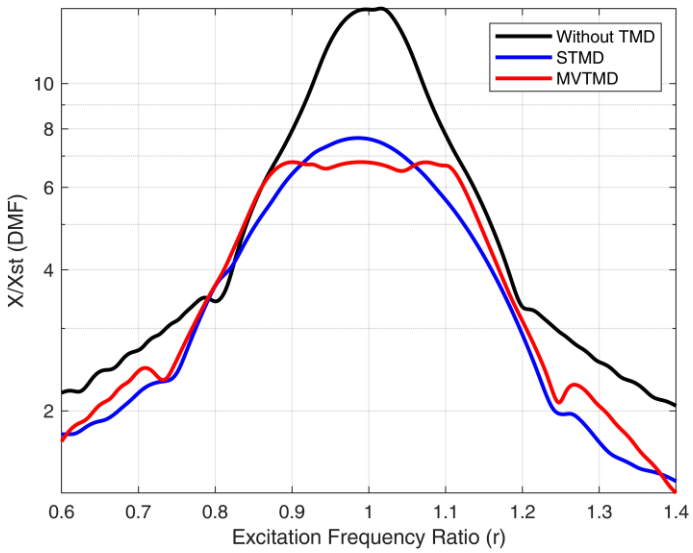

Figure 25. Relation between DMF and r for different TMD systems under six-parameter optimization for a 50-story building

The optimization results for the five-story presented in Table 6 and illustrated in Figure 17 to Figure 19 indicate the performance of the proposed MVTMD system under different parameter optimization scenarios. For the eight-parameter optimization case, the minimum dynamic magnification factor (DMF) obtained was 5.06881. The corresponding reduction in structural response was 80.20% compared to the uncontrolled structure and approximately 12.90% compared to the optimal Single Tuned Mass Damper (STMD), as shown in Figure 17. When the total mass ratio was fixed at $\mu = 0.01$ in the seven-parameter optimization scenario, the minimum DMF increased to 7.18713. In this scenario, the structural response was reduced by 72.00% relative to the uncontrolled structure and by approximately 12.40% compared to the STMD, as illustrated in Figure 18. Further constraints applied in the six-parameter optimization, with both the total mass ratio ($\mu = 0.01$) and the number of tuned mass dampers (NTMD = 3) fixed, resulted in a slightly increased DMF of 7.20627. Here, the structural response was reduced by 71.90% relative to the uncontrolled case, providing approximately 12.10% improvement compared to the STMD configuration, as depicted in Figure 19.

The optimization results summarized in Table 7 and depicted in Figure 20 to Figure 22 present the performance of the proposed MVTMD system under different parameter optimization scenarios for the 25-story structure. The minimum dynamic magnification factor (DMF) obtained from the eight-parameter optimization was 5.04419. In this case, the structural response was reduced by 75.00% relative to the uncontrolled structure, corresponding to approximately 9.70% additional reduction compared to the optimal Single Tuned Mass Damper (STMD), as illustrated in Figure 20. In the seven-parameter optimization scenario, with the total mass ratio (μ) fixed at 0.01, the minimum DMF increased to 7.19818. Under these conditions, the MVTMD system reduced the structural response by 64.40% compared to the uncontrolled structure, achieving approximately 8.20% improvement over the STMD configuration, as shown in Figure 21. Further restricting optimization parameters in the six-parameter scenario, by fixing both the total mass ratio ($\mu = 0.01$) and the number of tuned mass dampers (NTMD = 3), resulted in a minimum DMF of 7.62178. In this configuration, the structural response was reduced by 62.30% compared to the uncontrolled structure, with approximately 2.80% improvement relative to the STMD, as indicated in Figure 22.

The optimization results summarized in Table 8 and illustrated in Figure 23 to Figure 25 indicate the performance of the proposed MVTMD system for the 50-story structure under three different optimization configurations. For the eight-parameter optimization case, the minimum dynamic magnification factor (DMF) obtained was 4.55949. This resulted in a structural response reduction of 68.60% compared to the uncontrolled structure and approximately 15.50% relative to the optimal Single Tuned Mass Damper (STMD) system, as observed in Figure 23. In the seven-parameter optimization scenario, where the total mass ratio was fixed at $\mu = 0.01$, the minimum DMF increased to 6.51581. This led to a structural response reduction of 55.20% compared to the uncontrolled case and an improvement of approximately 14.80% relative to the STMD configuration, as depicted in Figure 24. For the six-parameter optimization configuration, with both the total mass ratio ($\mu = 0.01$) and the number of tuned mass dampers (NTMD = 3) fixed, the minimum DMF reached 6.79455. The structural response was reduced by 53.20% compared to the uncontrolled case, with a reduction of approximately 11.20% relative to the STMD system, as shown in Figure 25.

Table 8. Optimal MVTMD system parameters derived from the genetic algorithm for the 50-story building

Trial	8 parameters	7 parameters	6 parameters
μ	0.02498	0.01	0.01
NTMD	16	19	3
μ_1	0.24111	0.40980	0.55019
f	0.94034	0.95671	0.95238
β	0.26292	0.15833	0.22018
ζ	0.04092	0.01850	0.04505
γ	0.65319	0.42320	0.99815
η	0.87382	1.34568	1.70288
DMF	4.55949	6.51581	6.79455

Several insights can be identified from the optimization results presented in Tables 6 to 8, which illustrate clear trends across different building heights and optimization scenarios. The optimum number of Tuned Mass Dampers (NTMD) consistently increases with building height, rising from 11 in the 5-story structure to 14 in the 25-story and 16 in the 50-story case under the eight-parameter optimization scenario. This trend clearly indicates that taller buildings necessitate a higher number of dampers for optimal vibration suppression. In the eight-parameter optimization, the optimal mass ratio (μ) enhances the effectiveness of the MVTMD, with higher mass ratios generally yielding improved vibration control, which aligns with the same conclusion reported by Mohebbi et al. [30] for MTMD system. The first mass ratio (μ_1) decreases slightly as building height increases, dropping from 0.29173 in the 5-story case to 0.26270 in the 25-story and 0.24111 in the 50-story structure. The optimal tuning ratio f remains relatively stable across different heights, generally fluctuating between approximately 0.94 and 0.96. The small variations observed suggest that the optimal tuning ratio is less sensitive to changes in building height. The frequency bandwidth parameter β does not show a clear height-dependent pattern but instead fluctuates slightly depending on the degree of parameter optimization, generally decreasing when fewer parameters are considered. Conversely, the viscoelastic coupling parameters γ and η exhibit a noticeable increase with building height, particularly in more flexible optimization scenarios, demonstrating the need for stronger viscoelastic connections in taller buildings. The damping ratio ζ, however, displays considerable variability across scenarios without a consistent relationship to structural height. In all cases, the MVTMD system generates flatter Dynamic Magnification Factor (DMF) curves with consistent peak responses and surpasses the optimal STMD by achieving greater displacement reductions.

4.3. Response of MVTMD to Earthquakes

The seismic performance of the proposed MVTMD system was further investigated by considering the building model whose structural properties are summarized in Table 5. The structure was subjected to three benchmark earthquake records El Centro, Loma Prieta, and Northridge employing the MVTMD configuration optimized over the full set of eight design parameters. For the five-story building, structural responses under these earthquakes are depicted in Figure 26 to Figure 28, each comprising two subplots: (a) top-floor lateral displacement time histories and (b) maximum displacement distributions across all stories. Comparative analysis demonstrates that the structure with MVTMD consistently outperformed both the uncontrolled structure and the structure with optimal STMD. As illustrated in Figure 26, under the El Centro earthquake the MVTMD achieved a reduction of 11.20% in the top-floor displacement, compared with 10.50% obtained by the STMD. As shown in Figure 27, under the Loma Prieta earthquake the MVTMD produced a markedly greater reduction of 46.30%, whereas the STMD attained 44.90%. As shown in Figure 28, for the Northridge earthquake the performance of the MVTMD was nearly identical to that of the STMD, with both systems achieving a displacement reduction of approximately 12.50%.

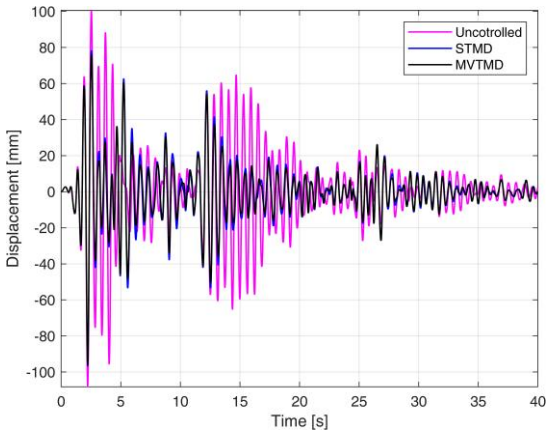

(a) Top-floor displacement time history

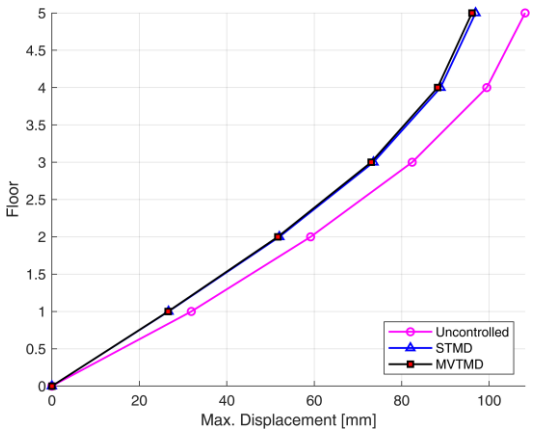

(b) Maximum displacement distribution across stories

Figure 26. Structural response of the five-story building under the El Centro earthquake: (a) top-floor displacement time history; (b) maximum displacement distribution across stories

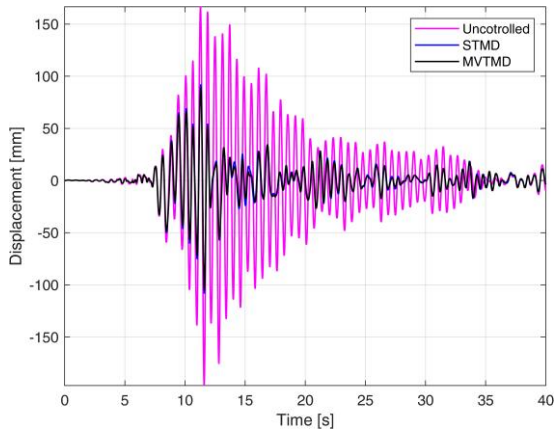

(a) Top-floor displacement time history

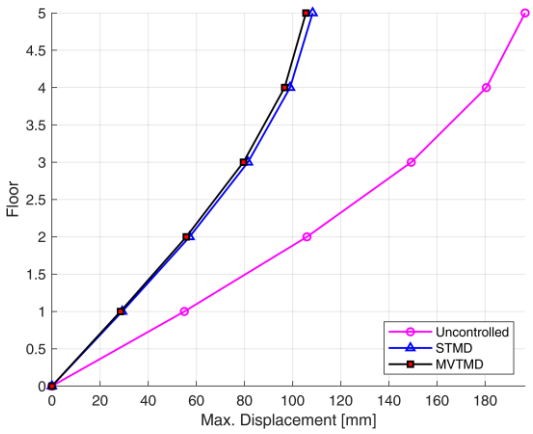

(b) Maximum displacement distribution across stories

Figure 27. Structural response of the five-story building under the Loma Prieta earthquake: (a) top-floor displacement time history; (b) maximum displacement distribution across stories

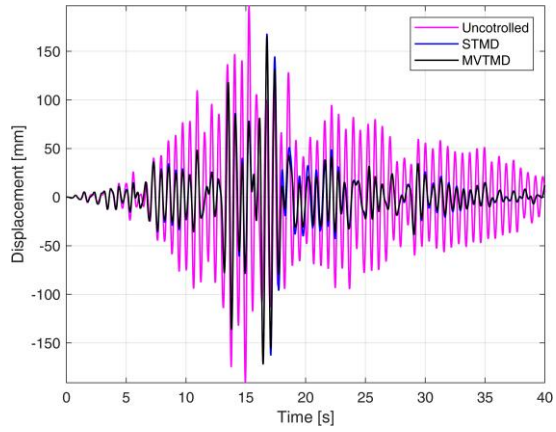

(a) Top-floor displacement time history

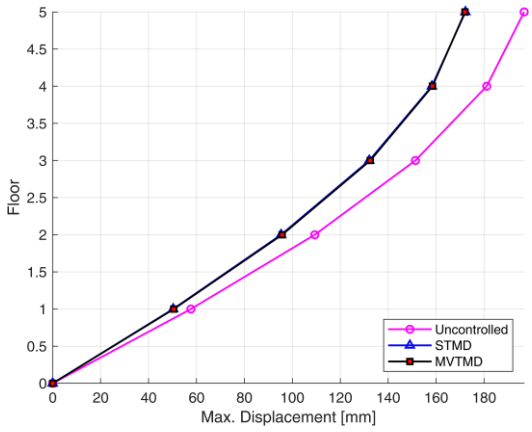

(b) Maximum displacement distribution across stories

Figure 28. Structural response of the five-story building under the Northridge earthquake: (a) top-floor displacement time history; (b) maximum displacement distribution across stories

For the twenty-five-story building, the corresponding structural responses are presented in Figure 29 to Figure 31, each comprising two subplots: (a) the time history of the top-floor lateral displacement, and (b) the distribution of the maximum displacement across all stories. The comparative results clearly indicate that the structure equipped with the MVTMD consistently exhibited superior seismic performance relative to both the uncontrolled structure and the structure controlled by the optimal STMD. As illustrated in Figure 29, under the El Centro earthquake the MVTMD achieved a reduction of approximately 15.60% in the top-floor displacement, compared with 14.70% obtained by the STMD. As shown in Figure 30, under the Loma Prieta earthquake the MVTMD attained a reduction of 29.70%, marginally outperforming the STMD, which yielded 29.40%. As shown in Figure 31, for the Northridge earthquake the MVTMD demonstrated a more pronounced improvement, achieving a displacement reduction of 4.90%, compared with 3.80% obtained by the optimal STMD.

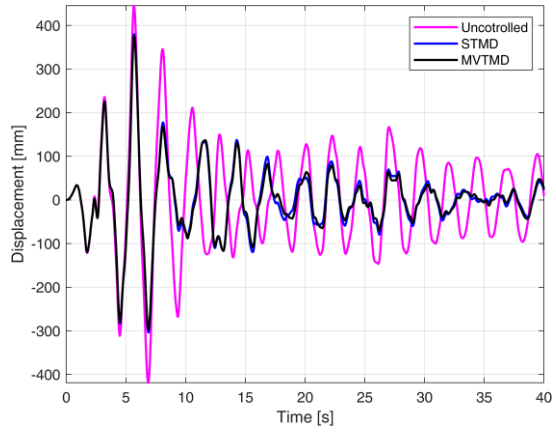

(a) Top-floor displacement time history

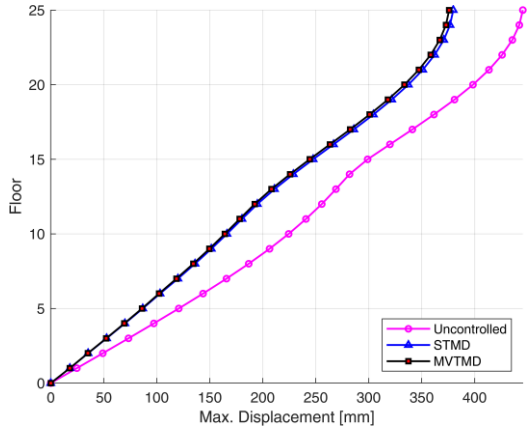

(b) Maximum displacement distribution across stories

Figure 29. Structural response of the twenty-five-story building under the El Centro earthquake: (a) top-floor displacement time history; (b) maximum displacement distribution across stories

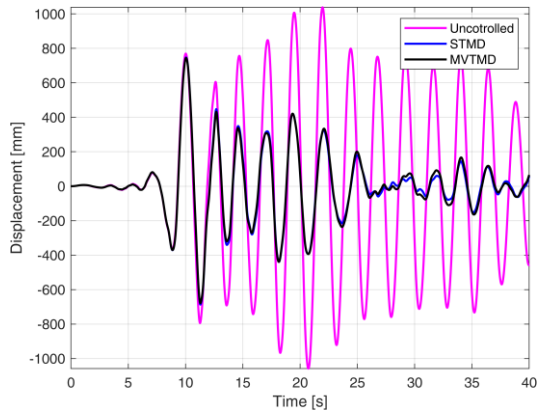

(a) Top-floor displacement time history

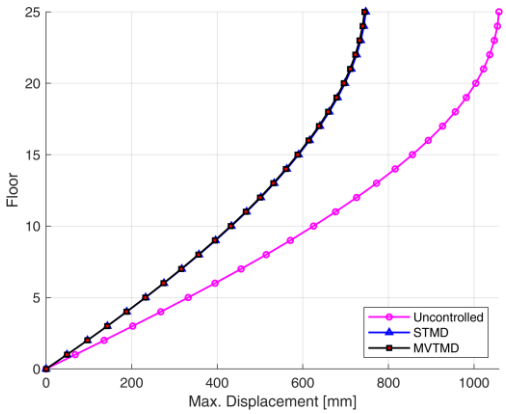

(b) Maximum displacement distribution across stories

Figure 30. Structural response of the twenty-five-story building under the Loma Prieta earthquake: (a) top-floor displacement time history; (b) maximum displacement distribution across stories

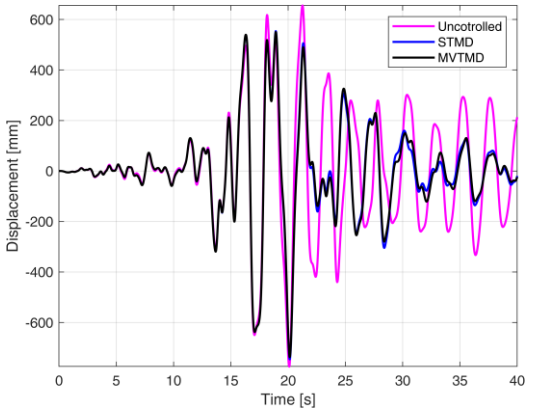

(a) Top-floor displacement time history

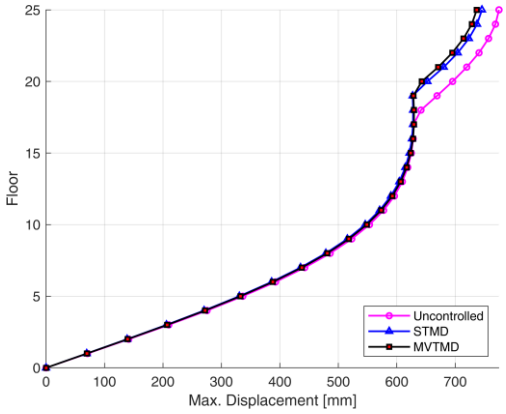

(b) Maximum displacement distribution across stories

Figure 31. Structural response of the twenty-five-story building under the Northridge earthquake: (a) top-floor displacement time history; (b) maximum displacement distribution across stories

For the fifty-story building, the corresponding structural responses are presented in Figures 32 to 34, each comprising two subplots: (a) the time history of the top-floor lateral displacement, and (b) the distribution of the maximum displacement across all stories. The comparative results clearly indicate that the structure equipped with the MVTMD consistently exhibited superior seismic performance relative to both the uncontrolled structure and the structure controlled by the optimal STMD. As illustrated in Figure 32, under the El Centro earthquake the MVTMD achieved a reduction of approximately 4.90% in the top-floor displacement, marginally below the 5.00% obtained by the STMD. As shown in Figure 33, under the Loma Prieta earthquake the MVTMD attained a reduction of 25.10%, clearly outperforming the STMD, which yielded 22.70%. As shown in Figure 34, for the Northridge earthquake the performance of the MVTMD was nearly identical to that of the STMD, with both systems achieving a displacement reduction of approximately 7.00%. Considered alongside the five- and twenty-five-story results, these findings confirm that the MVTMD remains effective across low-, mid-, and high-rise structures and under a diverse set of seismic excitations, with its advantage over the STMD becoming most pronounced for records exhibiting strong frequency content.

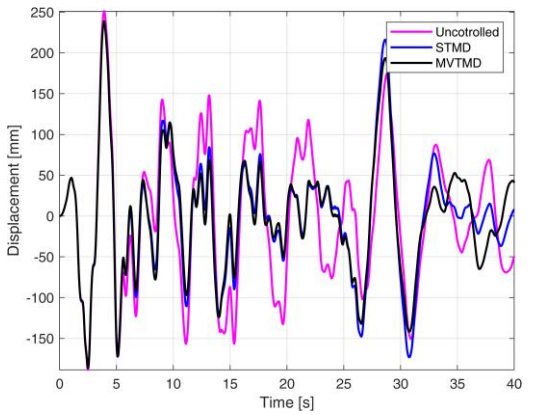

(a) Top-floor displacement time history

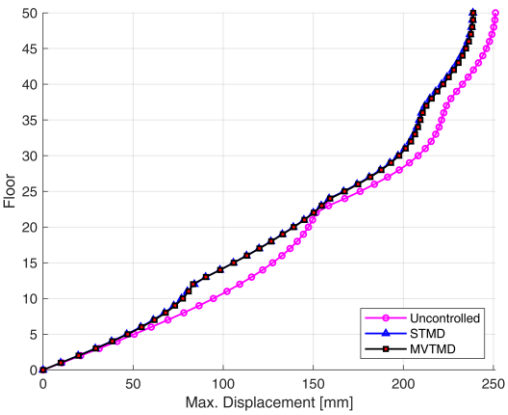

(b) Maximum displacement distribution across stories

Figure 32. Structural response of the fifty-story building under the El Centro earthquake: (a) top-floor displacement time history; (b) maximum displacement distribution across stories

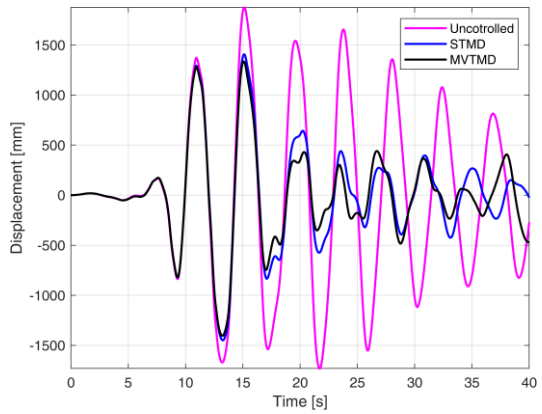

(a) Top-floor displacement time history

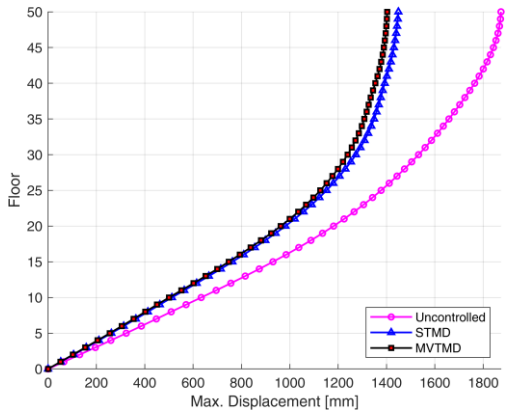

(b) Maximum displacement distribution across stories

Figure 33. Structural response of the fifty-story building under the Loma Prieta earthquake: (a) top-floor displacement time history; (b) maximum displacement distribution across stories

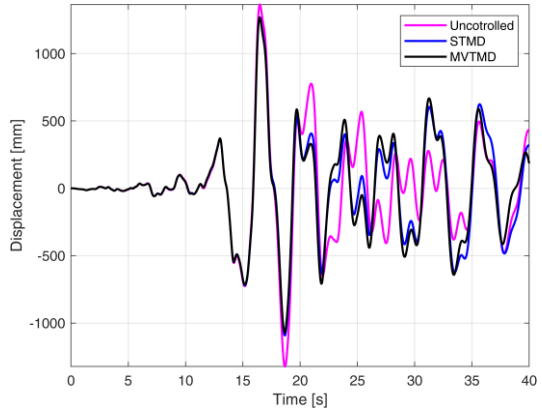

(a) Top-floor displacement time history

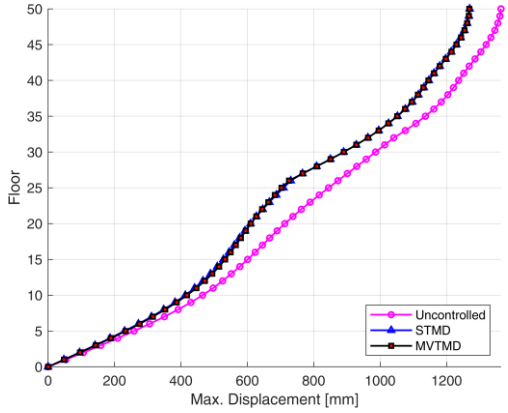

(b) Maximum displacement distribution across stories

Figure 34. Structural response of the fifty-story building under the Northridge earthquake: (a) top-floor displacement time history; (b) maximum displacement distribution across stories

5. Conclusions

In this study, a novel Multiple Viscoelastic-Connected Tuned Mass Damper (MVTMD) system was proposed to reduce structural vibrations caused by wind and earthquakes. A thorough parametric analysis was performed to identify key parameters influencing the system's performance. Due to the inherent complexity and interdependencies of these parameters, an optimization was efficiently performed using a real-coded genetic algorithm. The optimized MVTMD system demonstrated superior vibration control performance compared to a conventional Single Tuned Mass Damper (STMD). The main findings of the study can be summarized as follows:

- The MVTMD consistently outperformed the optimal STMD, achieving flatter DMF curves and greater displacement reductions across all cases.
- Under full (8-parameter) optimization, substantial displacement reductions of 80.20%, 75.00%, and 68.60% relative to the original building were achieved for the five-, twenty-five-, and fifty-story buildings, respectively.
- The MVTMD system consistently exhibited superior displacement reductions over the optimal STMD across all investigated scenarios. Specifically, the system achieved additional displacement reductions of 12.90%, 9.70%, and 15.50% for the five-, twenty-five-, and fifty-story structures, respectively.
- The optimization results reveal that taller buildings require more TMDs, rising from 11 (5-story) to 16 (50-story), and stronger viscoelastic coupling (γ, η) to maintain control effectiveness. While the tuning ratio f remained stable (0.94 to 0.96), the first mass ratio μ_1 decreased from 0.29173 to 0.24111 with height.
- Under various earthquake scenarios, the MVTMD consistently decreased top-floor and interstory displacements across all building heights. The most pronounced improvements were observed in the 25-story building, showing displacement reductions up to 4% better than STMD, while the 5-story structure exhibited a maximum reduction of 46.30% under the Loma Prieta earthquake.

Overall, the findings confirm that the proposed MVTMD system is robust, highly adaptable, and provides significant performance advantages over traditional STMD across various building heights and loading conditions. Future research directions may include exploring multiple optimization methods, extending the proposed MVTMD concept into semi-active control systems, and conducting further validation through experimental studies and full-scale implementations.

6. Declarations

6.1. Author Contributions

Conceptualization, M.B. and T.A.S.; methodology, T.A.S.; software, M.B.; validation, M.B. and T.A.S.; formal analysis, M.B.; investigation, M.B.; resources, T.A.S. and M.S.; data curation T.A.S. and M.S.; writing—original draft preparation, M.B.; writing—review and editing, T.A.S. and M.S.; visualization M.B. and T.A.S.; supervision, T.A.S.; project administration, T.A.S. All authors have read and agreed to the published version of the manuscript.

6.2. Data Availability Statement

The data presented in this study are available in the article.

6.3. Funding

The authors received no financial support for the research, authorship, and/or publication of this article.

6.4. Conflicts of Interest

The authors declare no conflict of interest.

7. References

[1] Frahm, H. (1911). Device for damping vibrations of bodies. U.S. Patent No. 989,958, United States Patent and Trademark Office, Washington, United States.

[2] Ormondroyd, J., & Den Hartog, J. P. (1928). The Theory of the Dynamic Vibration Absorber. Transactions of the American Society of Mechanical Engineers, 49-50(2), 4058553. doi:10.1115/1.4058553.

[3] Den Hartog, J. P. (1985). Mechanical vibrations. Courier Corporation, North Chelmsford, United States.

[4] Lago, A., Trabucco, D., & Wood, A. (2018). Damping Technologies for Tall Buildings: Theory, Design Guidance and Case Studies. Butterworth-Heinemann, Oxford, United Kingdom. doi:10.1016/C2017-0-01327-7.

[5] Tuan, A. Y., & Shang, G. Q. (2014). Vibration control in a 101-storey building using a tuned mass damper. Journal of Applied Science and Engineering, 17(2), 141–156. doi:10.6180/jase.2014.17.2.05.

[6] Elias, S., & Matsagar, V. (2017). Research developments in vibration control of structures using passive tuned mass dampers. Annual Reviews in Control, 44, 129–156. doi:10.1016/j.arcontrol.2017.09.015.

[7] CTBUH. (2018). World's Tallest Buildings with Dampers. CTBUH Journal 2018(Issue III): 48, Council on Tall Buildings and Urban Habitat (CTBUH), Chicago, United States.

[8] Yang, F., Sedaghati, R., & Esmailzadeh, E. (2022). Vibration suppression of structures using tuned mass damper technology: A state-of-the-art review. JVC/Journal of Vibration and Control, 28(7–8), 812–836. doi:10.1177/1077546320984305.

[9] Çelebi, O., & Aydın, A. C. (2025). A review on the Control Systems Developed for Earthquake Controlled Structures. Iranian Journal of Science and Technology - Transactions of Civil Engineering, 49(3), 2139–2171. doi:10.1007/s40996-024-01514-6.

[10] Brock, J. E. (1946). A Note on the Damped Vibration Absorber. Journal of Applied Mechanics, 13(4), A284–A284. doi:10.1115/1.4009588.

[11] Snowdon, J. C. (1959). Steady-State Behavior of the Dynamic Absorber. The Journal of the Acoustical Society of America, 31(8), 1096–1103. doi:10.1121/1.1907832.

[12] Crandall, S. H., & Mark, W. D. (2014). Random vibration in mechanical systems. Academic Press, Cambridge, United States.

[13] Falcon, K. C., Stone, B. J., Simcock, W. D., & Andrew, C. (1967). Optimization of Vibration Absorbers: A Graphical Method for use on Idealized Systems with Restricted Damping. Journal of Mechanical Engineering Science, 9(5), 374–381. doi:10.1243/jmes_jour_1967_009_058_02.

[14] Warburton, G. B., & Ayorinde, E. O. (1980). Optimum absorber parameters for simple systems. Earthquake Engineering & Structural Dynamics, 8(3), 197–217. doi:10.1002/eqe.4290080302.

[15] Thompson, A. G. (1981). Optimum tuning and damping of a dynamic vibration absorber applied to a force excited and damped primary system. Journal of Sound and Vibration, 77(3), 403–415. doi:10.1016/S0022-460X(81)80176-9.

[16] Warburton, G. B. (1982). Optimum absorber parameters for various combinations of response and excitation parameters. Earthquake Engineering & Structural Dynamics, 10(3), 381–401. doi:10.1002/eqe.4290100304.

[17] Tsai, H. -C, & Lin, G. -C. (1993). Optimum tuned-mass dampers for minimizing steady-state response of support-excited and damped systems. Earthquake Engineering & Structural Dynamics, 22(11), 957–973. doi:10.1002/eqe.4290221104.

[18] Sadek, F., Mohraz, B., Taylor, A. W., & Chung, R. M. (1997). A method of estimating the parameters of tuned mass dampers for seismic applications. Earthquake Engineering and Structural Dynamics, 26(6), 617–635. doi:10.1002/(SICI)1096-9845(199706)26:6<617::AID-EQE664>3.0.CO;2-Z.

[19] Rana, R., & Soong, T. T. (1998). Parametric study and simplified design of tuned mass dampers. Engineering Structures, 20(3), 193–204. doi:10.1016/S0141-0296(97)00078-3.

[20] Leung, A. Y. T., & Zhang, H. (2009). Particle swarm optimization of tuned mass dampers. Engineering Structures, 31(3), 715–728. doi:10.1016/j.engstruct.2008.11.017.

[21] ekdaş, G., & Nigdeli, S. M. (2011). Estimating optimum parameters of tuned mass dampers using harmony search. Engineering Structures, 33(9), 2716–2723. doi:10.1016/j.engstruct.2011.05.024.

[22] Arfiadi, Y., & Hadi, M. N. S. (2011). Optimum Placement and Properties of Tuned Mass Dampers Using Hybrid Genetic Algorithms. International Journal of Optimization in Civil Engineering, 1(September), 167–187.

[23] Xu, K., & Igusa, T. (1992). Dynamic characteristics of multiple substructures with closely spaced frequencies. Earthquake Engineering & Structural Dynamics, 21(12), 1059–1070. doi:10.1002/eqe.4290211203.

[24] Yamaguchi, H., & Harnpornchai, N. (1993). Fundamental characteristics of Multiple Tuned Mass Dampers for suppressing harmonically forced oscillations. Earthquake Engineering & Structural Dynamics, 22(1), 51–62. doi:10.1002/eqe.4290220105.

[25] Kareem, A., & Kline, S. (1995). Performance of Multiple Mass Dampers under Random Loading. Journal of Structural Engineering, 121(2), 348–361. doi:10.1061/(asce)0733-9445(1995)121:2(348).

[26] Li, C. (2000). Performance of multiple tuned mass dampers for attenuating undesirable oscillations of structures under the ground acceleration. Earthquake Engineering & Structural Dynamics, 29(9), 1405–1421. doi:10.1002/1096-9845(200009)29:9<1405::aid-eqe976>3.0.co;2-4.

[27] Li, C., & Liu, Y. (2003). Optimum multiple tuned mass dampers for structures under the ground acceleration based on the uniform distribution of system parameters. Earthquake Engineering and Structural Dynamics, 32(5), 671-690. doi:10.1002/eqe.239.

[28] Zuo, L., & Nayfeh, S. A. (2004). Minimax optimization of multi-degree-of-freedom tuned-mass dampers. Journal of Sound and Vibration, 272(3–5), 893–908. doi:10.1016/S0022-460X(03)00500-5.

[29] Lee, C. L., Chen, Y. T., Chung, L. L., & Wang, Y. P. (2006). Optimal design theories and applications of tuned mass dampers. Engineering Structures, 28(1), 43–53. doi:10.1016/j.engstruct.2005.06.023.

[30] Mohebbi, M., Shakeri, K., Ghanbarpour, Y., & Majzoub, H. (2013). Designing optimal multiple tuned mass dampers using genetic algorithms (GAs) for mitigating the seismic response of structures. JVC/Journal of Vibration and Control, 19(4), 605–625. doi:10.1177/1077546311434520.

[31] Wang, L., Zhou, Y., & Shi, W. (2024). Seismic multi-objective stochastic parameters optimization of multiple tuned mass damper system for a large podium twin towers structure. Soil Dynamics and Earthquake Engineering, 177, 108428. doi:10.1016/j.soildyn.2023.108428.

[32] Djerouni, S., Bekdaş, G., & Nigdeli, S. M. (2025). Optimization and performance assessment of Multi-Tuned Mass Dampers (MTMD) to mitigate seismic pounding of adjacent buildings via a novel hybrid algorithm. Journal of Building Engineering, 103, 112168. doi:10.1016/j.jobe.2025.112168.

[33] Domizio, M., Garrido, H., & Ambrosini, D. (2022). Single and multiple TMD optimization to control seismic response of nonlinear structures. Engineering Structures, 252, 113667. doi:10.1016/j.engstruct.2021.113667.

[34] Lara-Valencia, L., Echavarria-Montaña, S., & Valencia-Gonzalez, Y. (2024). Performance of multiple tuned inerter dampers optimized by a cultural algorithm to control response in buildings subjected to ground acceleration. Journal of Building Engineering, 92, 109537. doi:10.1016/j.jobe.2024.109537.

[35] Shahrouzi, M., Fahimi-Farzam, M., & Gholizadeh, J. (2025). Optimization of multiple tuned mass damper inerter by escaping bird search for seismic control of buildings. International Journal of Dynamics and Control, 13(10), 362. doi:10.1007/s40435-025-01875-4.

[36] Jafarinia, H., & Ostad-Ali-Askari, K. (2024). Optimum Setting Parameters of Multiple Tuned Mass Damper for Passive Control of Structures Using Cuckoo Algorithm. Iranian Journal of Science and Technology - Transactions of Civil Engineering, 48(3), 1483–1496. doi:10.1007/s40996-023-01233-4.

[37] Garrido, H., Curadelli, O., & Ambrosini, D. (2013). Improvement of tuned mass damper by using rotational inertia through tuned viscous mass damper. Engineering Structures, 56, 2149–2153. doi:10.1016/j.engstruct.2013.08.044.

[38] Li, L., Song, G., Singla, M., & Mo, Y. L. (2015). Vibration control of a traffic signal pole using a pounding tuned mass damper with viscoelastic materials (II): Experimental verification. JVC/Journal of Vibration and Control, 21(4), 670–675. doi:10.1177/1077546313488407.

[39] Berardengo, M., Cigada, A., Guanziroli, F., & Manzoni, S. (2015). Modelling and control of an adaptive tuned mass damper based on shape memory alloys and eddy currents. Journal of Sound and Vibration, 349, 18–38. doi:10.1016/j.jsv.2015.03.036.

[40] Sakr, T. A. (2017). Vibration control of buildings by using partial floor loads as multiple tuned mass dampers. HBRC Journal, 13(2), 133–144. doi:10.1016/j.hbrcj.2015.04.004.

[41] Liu, S., Li, H., Yang, J., Li, P., & Yang, S. (2025). Seismic analysis of a 20-story building with single and multi-tuned mass dampers including SSI effects. JVC/Journal of Vibration and Control, 32(7–8), 1782. doi:10.1177/10775463251321288.

[42] Araz, O., & Elias, S. (2024). Performance of differently arranged double-tuned mass dampers for structural seismic response control including soil-structure interaction. Engineering Structures, 319, 118841. doi:10.1016/j.engstruct.2024.118841.

[43] Araz, O. (2024). Effect of PGV/PGA ratio on seismic-induced vibrations of structures equipped with parallel tuned mass dampers considering SSI. Structures, 68, 107188. doi:10.1016/j.istruc.2024.107188.

[44] Ghaderi, P., & Farsijani, D. (2025). Torsional Behavior Enhancement of Asymmetric-Plan Building Structures Using Optimum Tuned Mass Damper Inerter. Journal of Earthquake Engineering, 29(3), 669–690. doi:10.1080/13632469.2024.2436109.

[45] Kiran, K. K., Al-Osta, M. A., Ahmad, S., & Bahraq, A. A. (2025). Optimal Design of Tuned Mass and Negative Stiffness Amplifier Dampers with Inerter by H2 Optimal Control Under Bidirectional Seismic Load. Arabian Journal for Science and Engineering, 50(3), 1753–1783. doi:10.1007/s13369-024-08960-4.

[46] Yang, Y., & Li, C. (2017). Performance of tuned tandem mass dampers for structures under the ground acceleration. Structural Control and Health Monitoring, 24(10), 1974. doi:10.1002/stc.1974.

[47] Batou, A., & Adhikari, S. (2019). Optimal parameters of viscoelastic tuned-mass dampers. Journal of Sound and Vibration, 445, 17–28. doi:10.1016/j.jsv.2019.01.010.

[48] Gai, P. P., Dai, J., Yang, Y., Bi, Q. S., Guan, Q. S., & Zhang, G. Y. (2025). Performance Enhancement of Seismically Protected Buildings Using Viscoelastic Tuned Inerter Damper. Actuators, 14(8), 360. doi:10.3390/act14080360.

[49] Chopra, A. K. (2007). Dynamics of structures. Pearson Education India, Chennai, India.

[50] Zhang, H., Li, A., Su, Y., Xu, G., & Sha, B. (2024). Viscoelastic dampers for civil engineering structures: A systematic review of constructions, materials, and applications. Journal of Building Engineering, 96. doi:10.1016/j.jobe.2024.110597.

[51] Gao, Z., Zhao, M., Wu, Y., Wang, M., & Du, X. (2023). Parameter design and performance evaluation of tuned mass damper (TMD) for seismic control of structure considering soil-structure interaction (SSI). Structures, 52, 1116–1129. doi:10.1016/j.istruc.2023.04.023.

[52] Wei, Z., Lv, M., Wu, S., Shen, M., Yan, M., Jia, S., Bao, Y., Han, P., & Zou, Z. (2022). Lateral Vibration Control of Long-Span Small-Radius Curved Steel Box Girder Pedestrian Bridge with Distributed Multiple Tuned Mass Dampers. Sensors, 22(12), 4329. doi:10.3390/s22124329.

[53] Haupt, R. L., & Haupt, S. E. (2004). Practical genetic algorithms. John Wiley & Sons, Hoboken, United States. doi:10.1002/0471671746.

[54] Khamis, A. (2024). Optimization Algorithms: AI techniques for design, planning, and control problems. Simon and Schuster, New York, United States.